Supplementary Information (SI) for Physical Chemistry Chemical Physics.

SUPPORTING INFORMATION

Two-dimensional $BiSbTeX_2$ (X = S, Se, Te) and their Janus monolayers as efficient thermoelectric materials

KM Sujata[1,2], Poonam Chauhan[1], Nidhi Verma[1], Rekha Garg Solanki[2]* and Ashok Kumar[1]*

[1]*Department of Physics, Central University of Punjab, Bathinda, India-151401*

[2]*Departmentof Physics, Dr. Hari Singh Gour University, Sagar, M.P., India-470003*

(October 8, 2024)

*Corresponding Authors: ashokphy@cup.edu.in (Ashok Kumar)

rgsolanki@dhsgsu.edu.in (Rekha Garg Solanki)

Geometrical structure and stability analysis

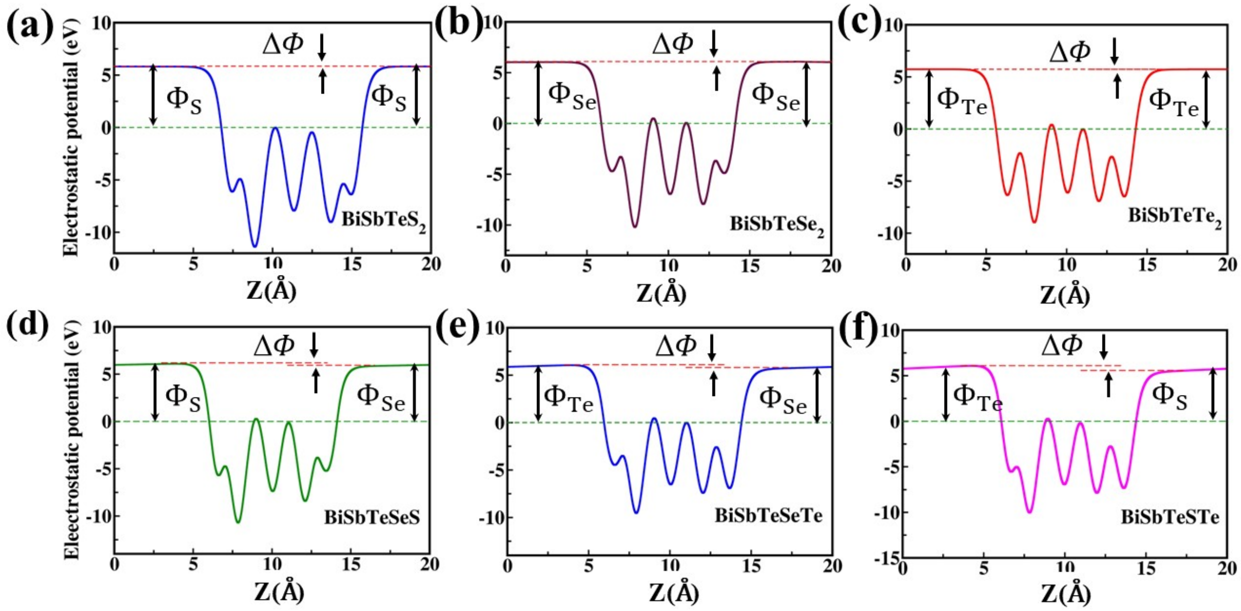

Fg. S1 Planar average of the electrostatic potential along the z axis of the **(a)-(b)** $BiSbTeX_2$ (X = S, Se, Te) and **(c)-(e)** Janus BiSbTeXY (X/Y = S, Se,Te) monolayers, respectively.

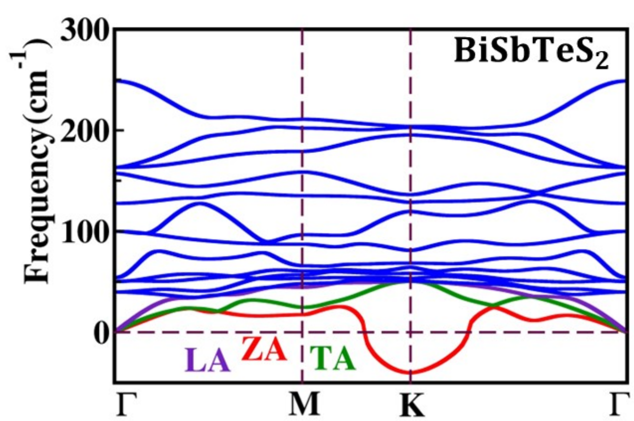

Fig. S2 Phonon dispersion curves with ZA, TA and LA accoustical mode of $BiSbTeS_2$ monolayer. This monolayer showing unstabilty due to ZA mode with negative frequency (-40.83 cm^{-1}) at K point.

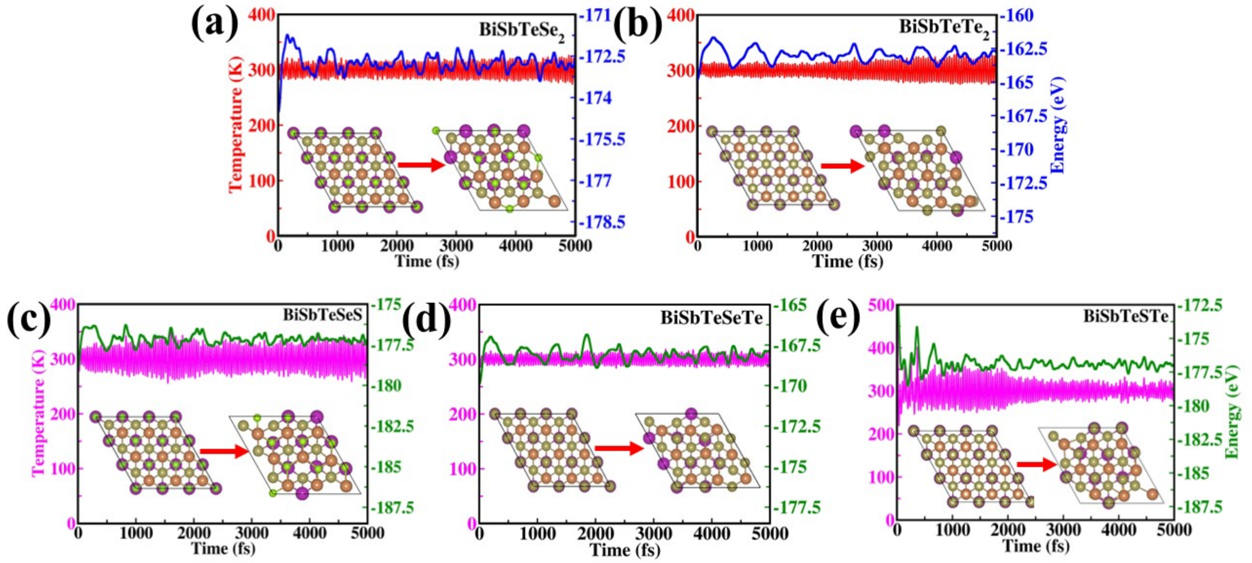

Fig. S3 The AIMD energy and temperature fluctuations at 300 K for **(a)-(b)** $BiSbTeX_2$ (X = Se, Te) monolayers and **(c)-(e)** Janus BiSbTeXY (X/Y = S, Se,Te) monolayers. The snapshot of the structures after 5000 fs AIMD simulations are also shown.

Electronic structure and mechanical response

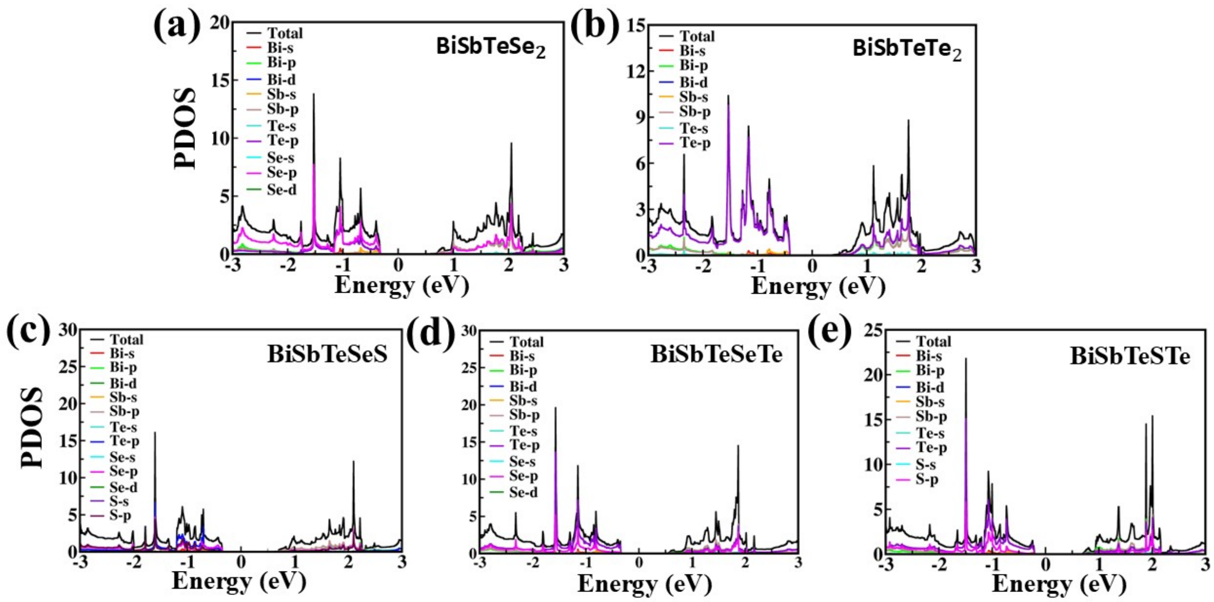

Fig. S4 The calculated PDOS using the PBE method of the (**a**)-(**b**) $BiSbTeX_2$ (X = Se, Te) and **(c)-(e)** Janus BiSbTeXY (X/Y = S, Se, Te) monolayers.

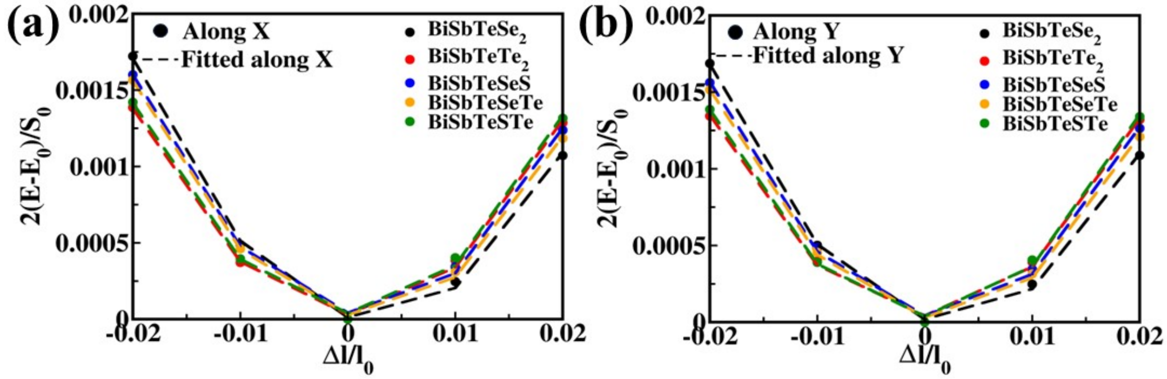

Fig. S5 Variation of **(a)-(b)** $\frac{2(E-E_0)}{S_0}$ w.r.t strain i.e. $\Delta l/l_0$ with their parabolic and linear fitting for elastic modulus. $(E-E_0)$ is the difference in the total energy of stable and strained structures, S_0 is the surface area of the $BiSbTeX_2$ (X = Se, Te) and Janus BiSbTeXY (X/Y = S, Se, Te) monolayers.

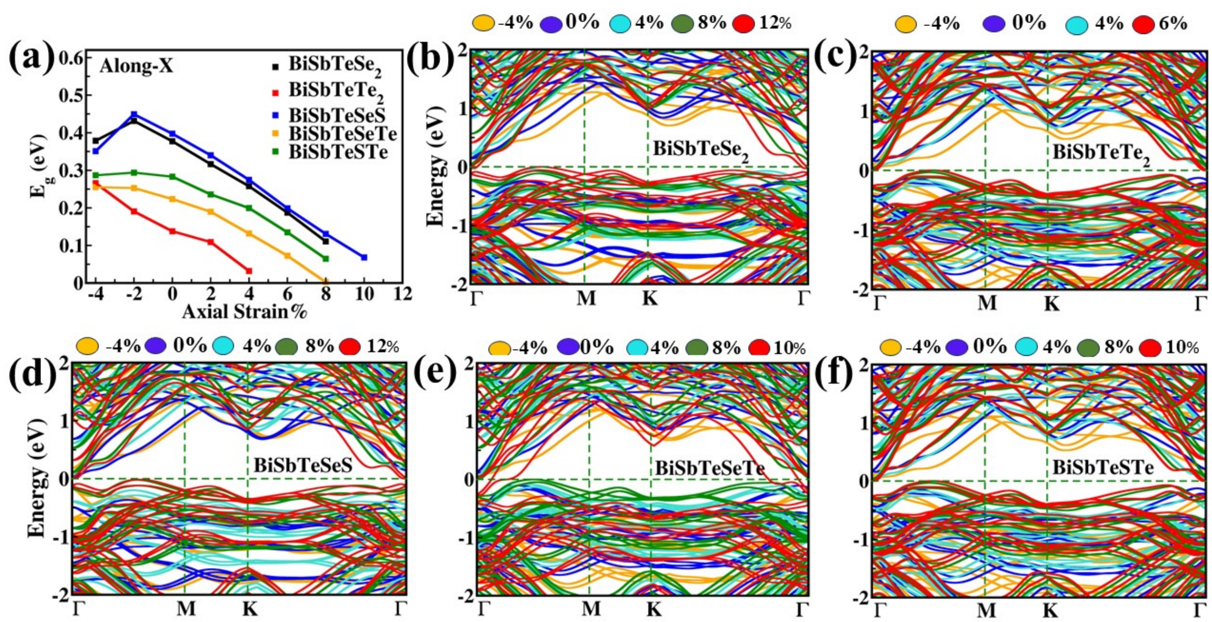

Fig. S6 (**a**) The evolution of bandgaps with axial strain, **(b)-(c)** band plot of the $BiSbTeX_2$ (X = Se, Te) and **(d)-(f)** Janus BiSbTeXY (X/Y = S, Se, Te) monolayers as a function of the applied uniaxial strains with the PBE+SOC method along x-direction.

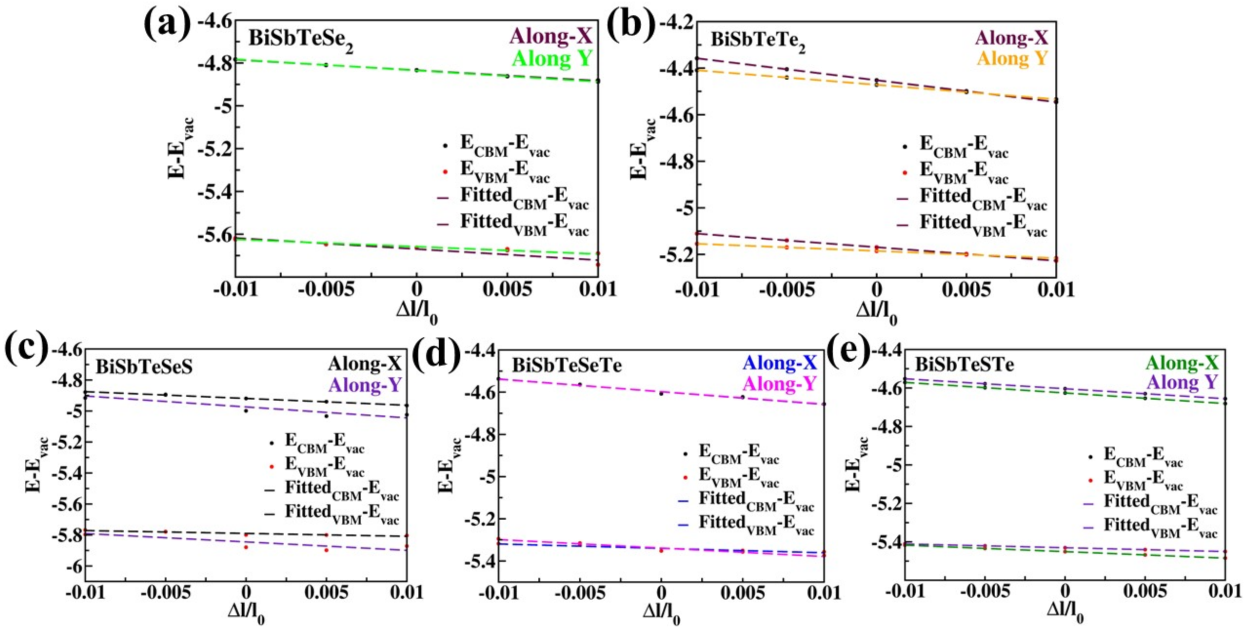

Fig.S7 Graph and straight fit graph between of E-E_{vac} and $\frac{\Delta l}{l_0}$ along X and Y direction, E-E_{vac} is the difference in the energy of i[th] band and vacuum energy, $\frac{\Delta l}{l_0}$ is the strain in the corresponding direction.

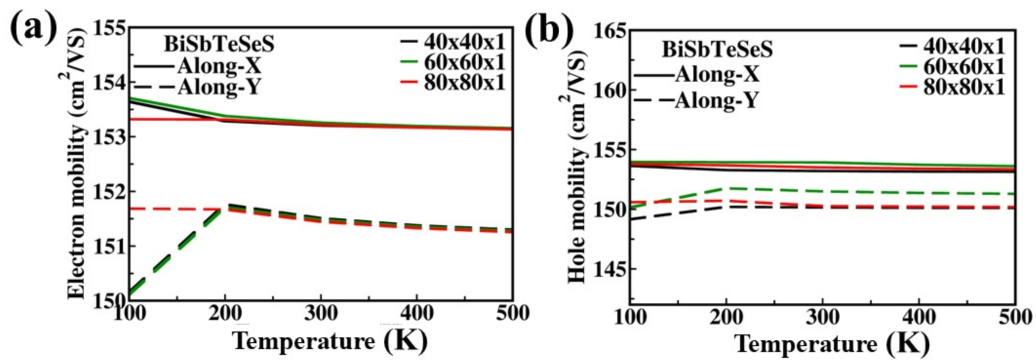

Fig.S8 Convergence test for the electron and hole mobilities of BiSbTeSeS at the different k- and q-mesh grids.

Table S1: The calculated values of m^*, m_d, E_d and μ_{2D} of 2D $BiSbTeX_2$ and Janus BiSbTeXY monolayers.

Materials	Carrier	m_X^*	m_Y^*	m_d	E_{d-X} (eV)	E_{d-Y} (eV)	μ_{2D-X} ($cm^2V^{-1}s^{-1}$)	μ_{2D-Y} ($cm^2V^{-1}s^{-1}$)
$BiSbTeSe_2$	electron	0.25	0.08	0.14	4.91	5.22	870	2380
	hole	1.38	0.81	1.05	5.18	3.43	20	70
$BiSbTeTe_2$	electron	0.09	0.21	0.13	9.39	6.25	640	620
	hole	0.37	0.15	0.23	5.83	3.09	240	2060
BiSbTeSeS	electron	0.09	0.16	0.12	4.38	7.07	3580	770
	hole	0.43	0.20	0.29	1.86	5.40	1700	430
BiSbTeSeTe	electron	0.25	0.40	0.31	6.02	5.92	240	160
	hole	0.87	0.15	0.36	2.09	4.01	510	820
BiSbTeSTe	electron	0.42	0.09	0.19	5.17	5.49	320	1350
	hole	0.43	0.19	0.28	1.99	3.37	1470	1160

Lattice thermal conductivity

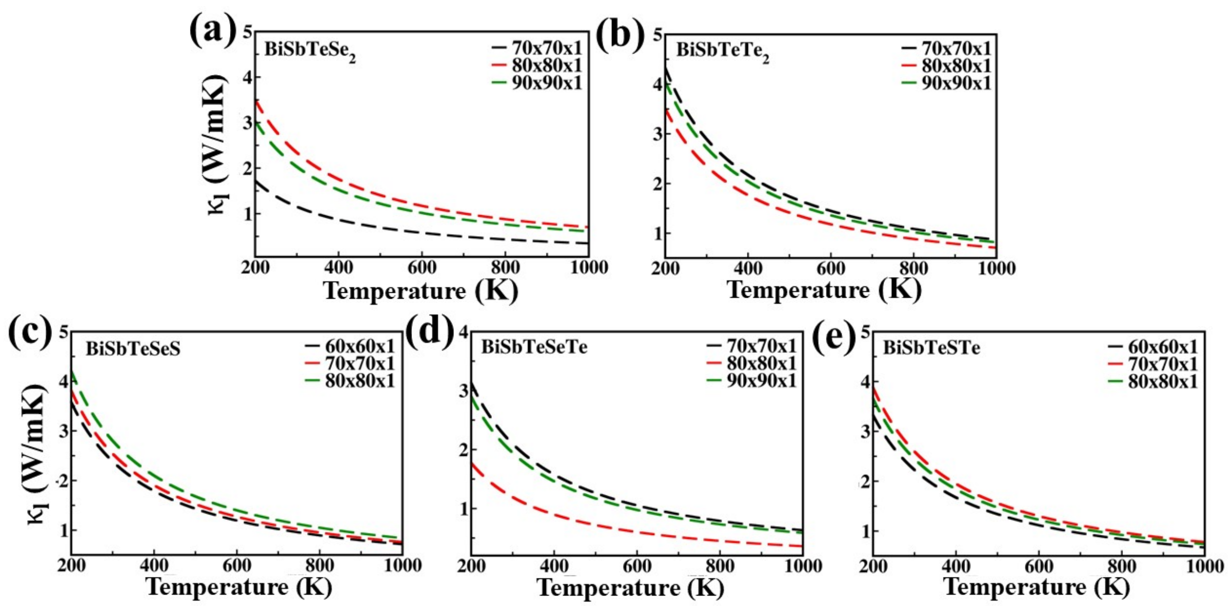

Fig. S9 The lattice thermal conductivities convergence at the different q-mesh grids of the **(a)-(b)** $BiSbTeX_2$ (X = Se, Te) and **(c)-(e)** Janus BiSbTeXY (X/Y = S, Se, Te). monolayers.

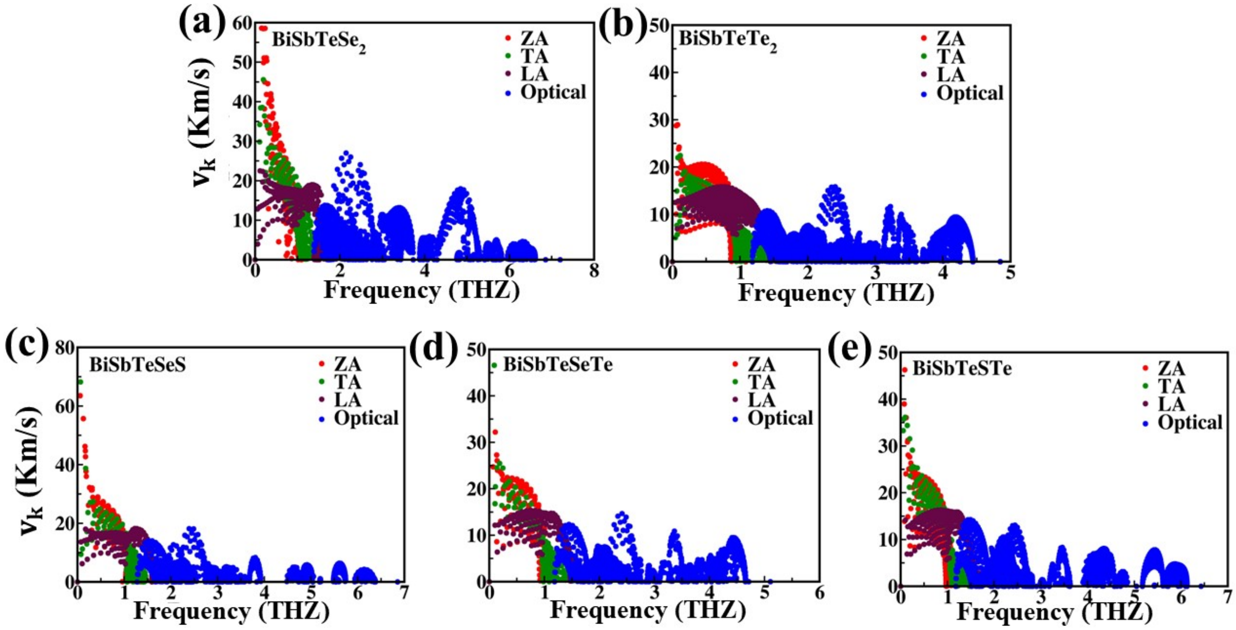

Fig. S10 The calculated group velocity for the $BiSbTeX_2$ (X = Se, Te) and Janus BiSbTeXY (X/Y = S, Se, Te). monolayers.

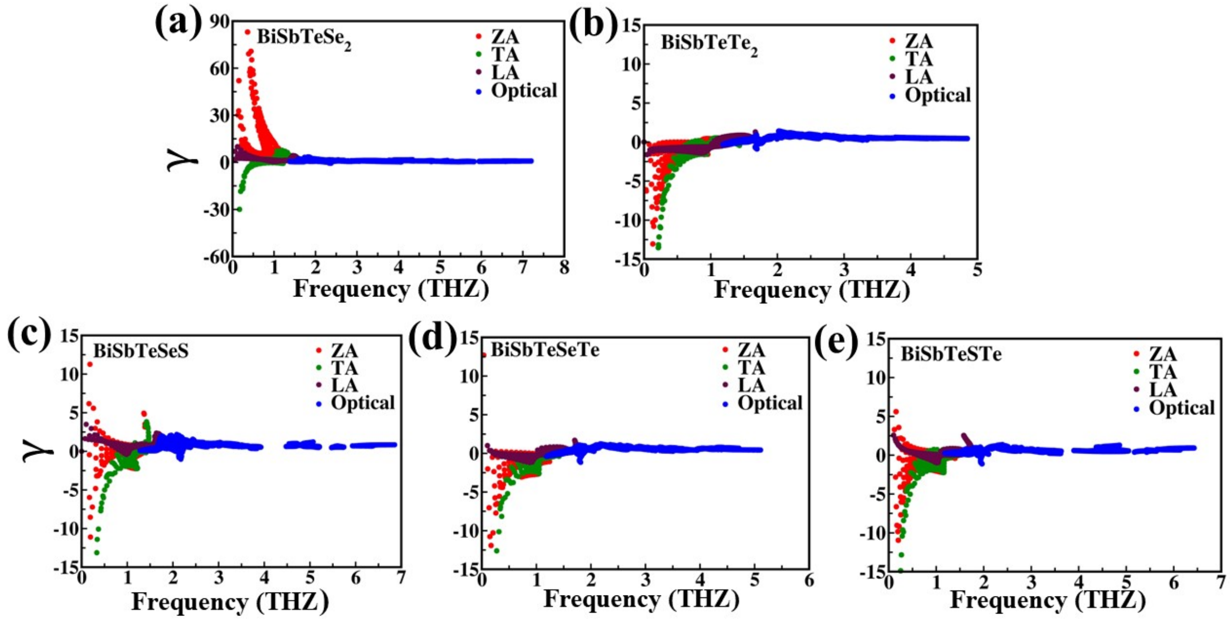

Fig. S11 The calculated Gruneisen parameter for the $BiSbTeX_2$ (X = Se, Te) and Janus BiSbTeXY (X/Y = S, Se, Te) monolayers.

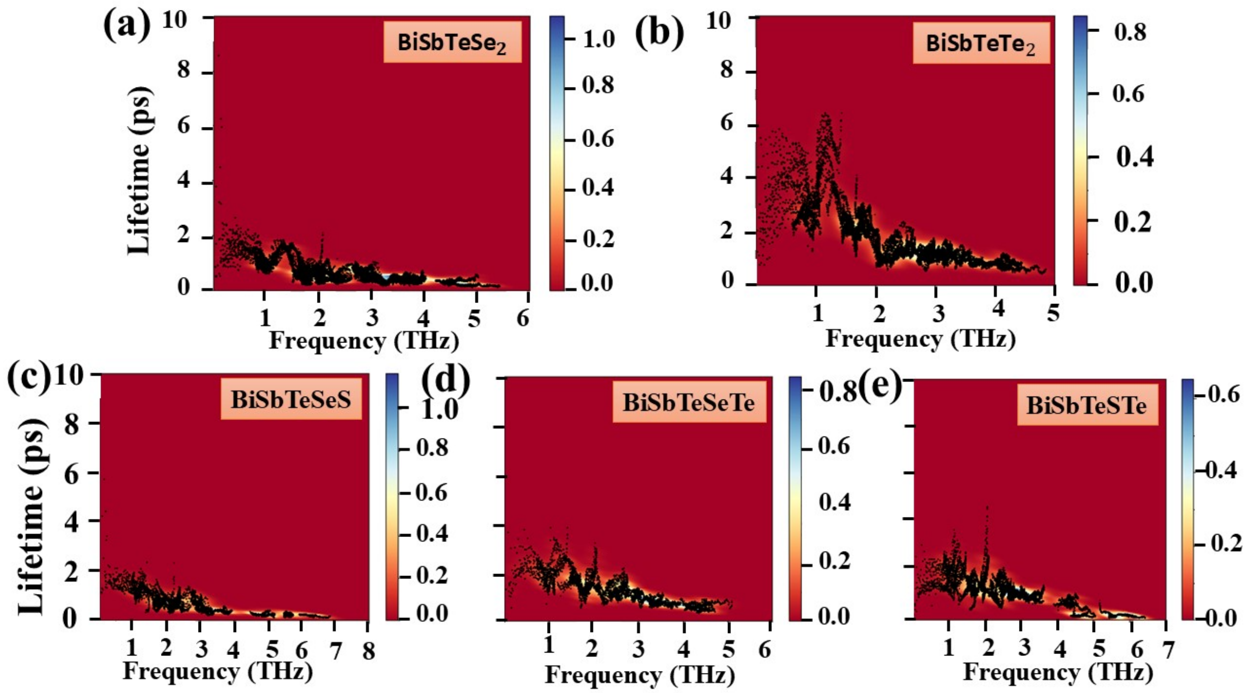

Fig. S12 Phonon life time plots for $BiSbTeX_2$ (X = Se, Te) and for Janus BiSbTeXY (X/Y = S, Se, Te) monolayers.

Electronic transport properties

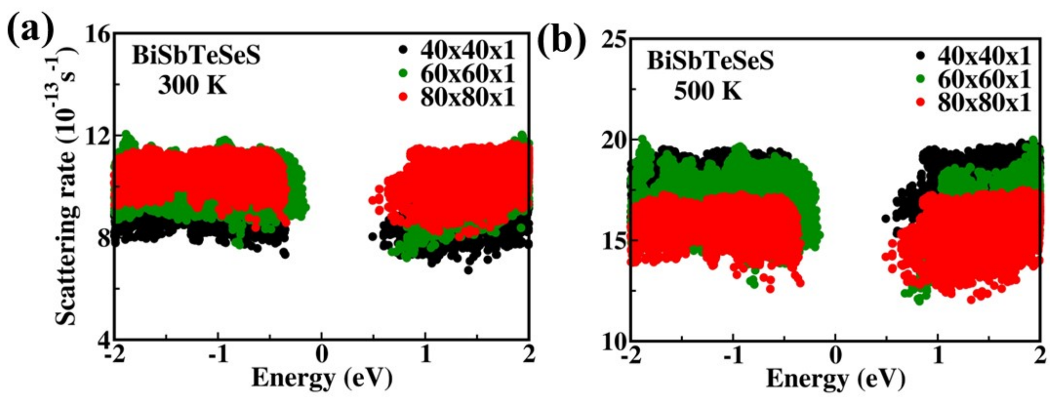

Fig. S13 The lattice thermal conductivities convergence at the different q-mesh grids of the **(a)-(b)** $BiSbTeX_2$ (X = Se, Te) and **(c)-(e)** Janus BiSbTeXY (X/Y = S, Se, Te) monolayers.

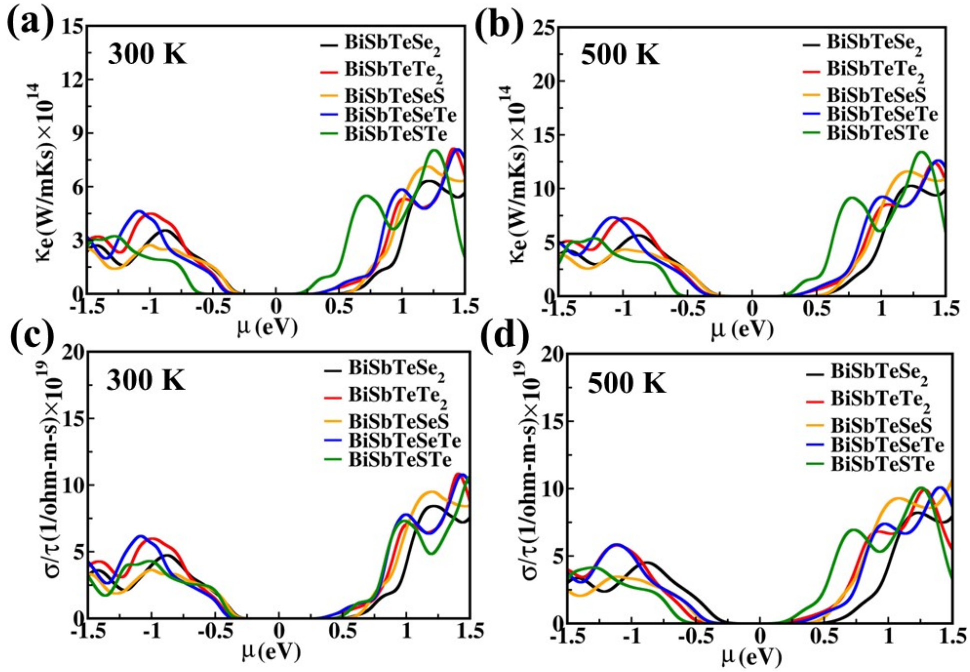

Fig. S14 The calculated **(a)-(b)** electronic thermal conductivity (κ_e/τ) and **(c)-(d)** electrical conductivity (σ/τ) with PBE method for p-type and n-type $BiSbTeX_2$ (X = Se, Te) and Janus BiSbTeXY (X/Y = S, Se, Te) monolayers at 300 K and 500 K temperature.

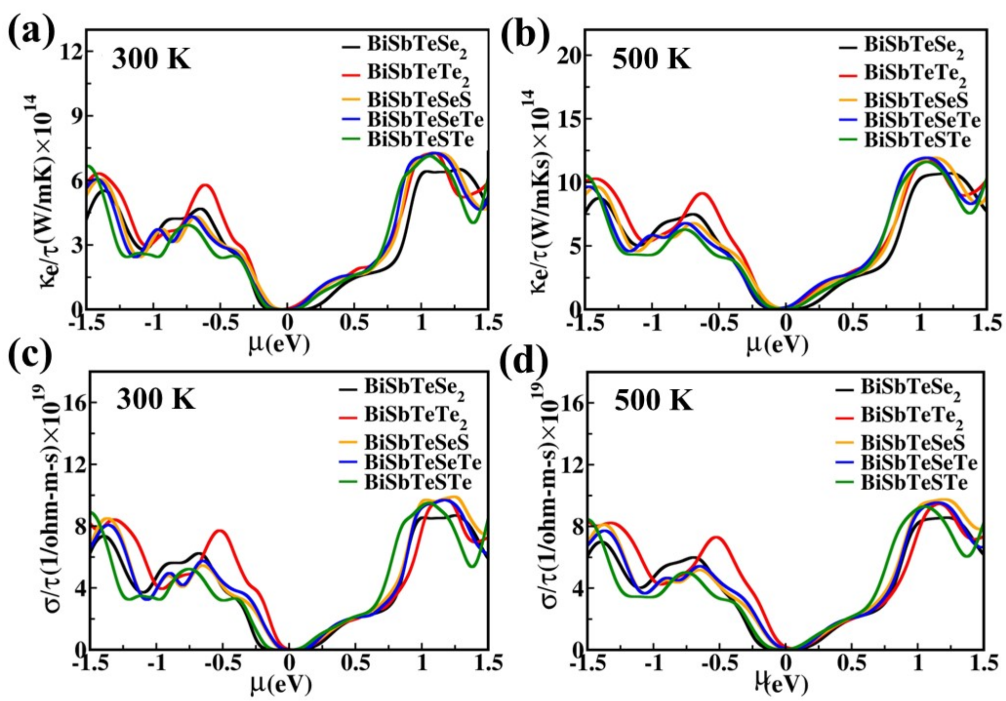

Fig. S15 The calculated **(a)-(b)** electronic thermal conductivity (κ_e/τ) and **(c)-(d)** electrical conductivity (σ/τ) with PBE+SOC method of $BiSbTeX_2$ (X = Se, Te) and Janus BiSbTeXY (X/Y = S, Se, Te) monolayers at 300 K and 500 K temperature.

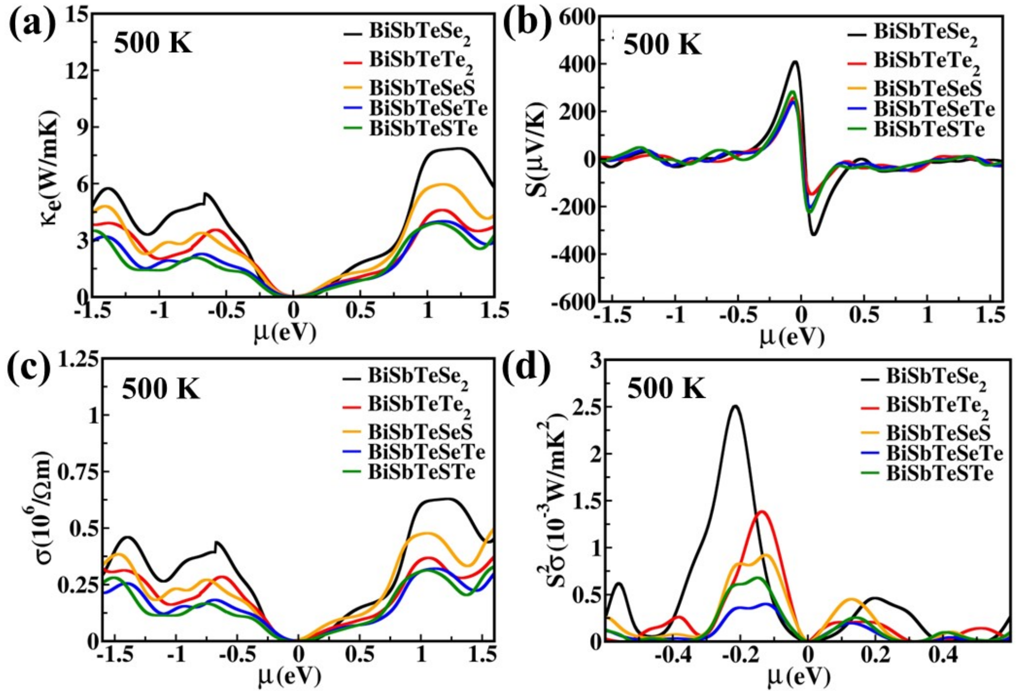

Fig. S16 The calculated **(a)** electronic thermal conductivity (κ_e), **(b)** Seebeck coefficient (S), **(c)** electrical conductivity (σ) and **(d)** Power factor ($S^2\sigma$) of $BiSbTeX_2$ (X=Se,Te) monolayers and Janus monolayers BiSbTeXY(X/Y=S,Se,Te) at 500K using PBE+SOC method.

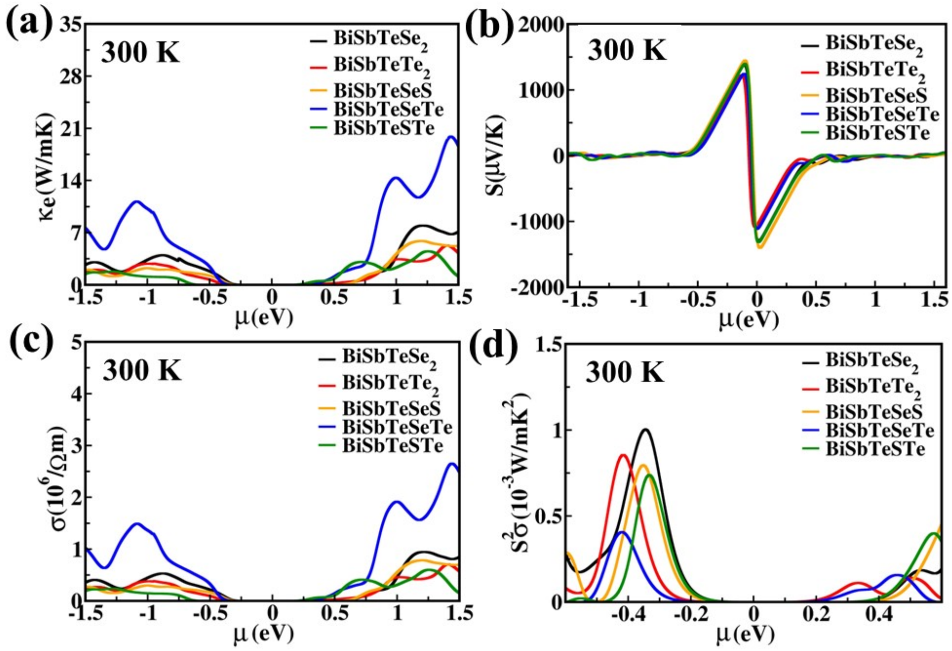

Fig. S17 The calculated **(a)** electronic thermal conductivity, **(b)** Seebeck coefficient, **(c)**, electrical conductivity and **(d)** Power factor of $BiSbTeX_2$ (X = Se, Te) and Janus BiSbTeXY (X/Y = S, Se, Te) monolayers at 300 K using PBE method.

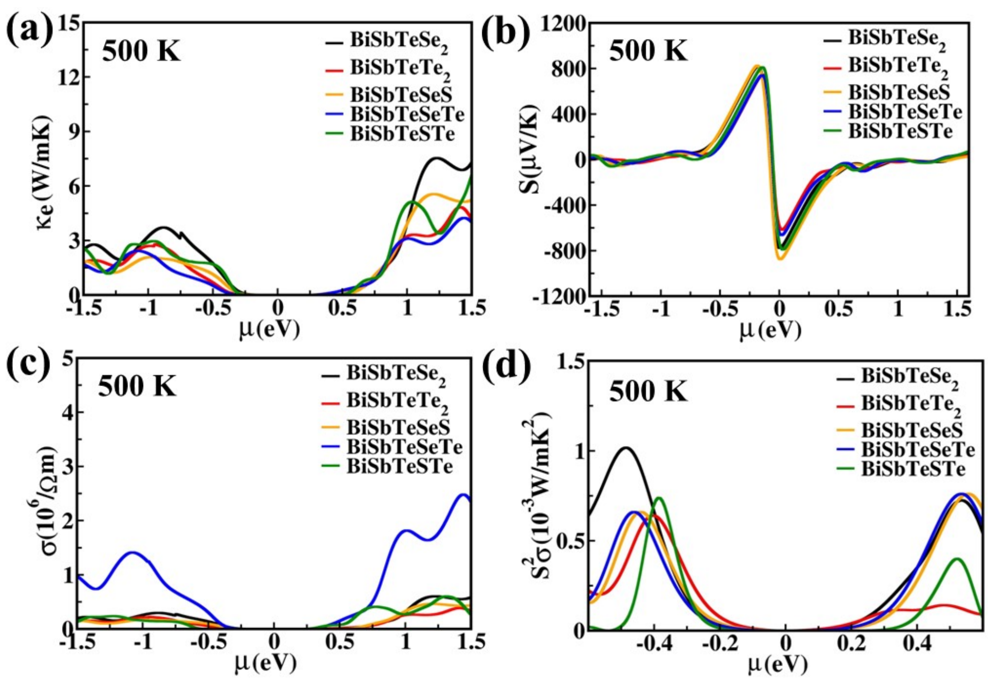

Fig. S18 The calculated **(a)** electronic thermal conductivity, **(b)** Seebeck coefficient, **(c)** electrical conductivity and **(d)** Power factor of $BiSbTeX_2$ (X = Se, Te) and Janus monolayers BiSbTeXY (X/Y = S, Se, Te) at 500K using PBE method.

Table S2: The calculated: Seebeck coefficient (S) of $BiSbTeX_2$ (X = Se, Te) and Janus monolayers BiSbTeXY (X/Y = S, Se, Te) using PBE and PBE+SOC method.

Materials	Carriers	S (μV/K)			
		PBE		PBE+SOC	
		300 K	500 K	300 K	500 K
$BiSbTeSe_2$	p-type	1383.90	821.37	658.24	411.34
	n-type	1290.35	774.21	554.98	318.85
$BiSbTeTe_2$	p-type	1227.03	745.18	359.34	256.34
	n-type	1088.66	612.86	232.28	223.61
BiSbTeSeS	p-type	1436.19	825.85	350.38	228.32
	n-type	1402.40	877.29	262.16	160.11
BiSbTeSeTe	p-type	1249.44	749.66	374.28	237.66
	n-type	1111.07	644.23	336.86	203.06
BiSbTeSTe	p-type	1398.84	812.41	440.01	282.48
	n-type	1312.76	792.13	396.621	225.48

Table S3: The calculated: power factor ($S^2\sigma$) of $BiSbTeX_2$ (X = Se, Te) and Janus monolayers BiSbTeXY (X/Y=S, Se, Te) with PBE method at 300 K temperature.

Materials	Carriers	$S^2\sigma \times 10^{-3} W/mK^2$)			
		PBE		PBE+SOC	
		300 K	500 K	300 K	500 K
$BiSbTeSe_2$	p-type	1.0	1.02	2.08	2.51
	n-type	0.80	0.73	0.47	0.47
$BiSbTeTe_2$	p-type	0.85	0.63	1.16	1.37
	n-type	0.11	0.11	0.24	0.21
BiSbTeSeS	p-type	0.80	0.66	0.47	0.91
	n-type	0.75	0.75	0.18	0.45
BiSbTeSeTe	p-type	0.87	0.66	0.63	0.40
	n-type	0.45	0.76	0.26	0.20
BiSbTeSTe	p-type	0.73	0.73	0.47	0.66
	n-type	0.40	0.40	0.18	0.25

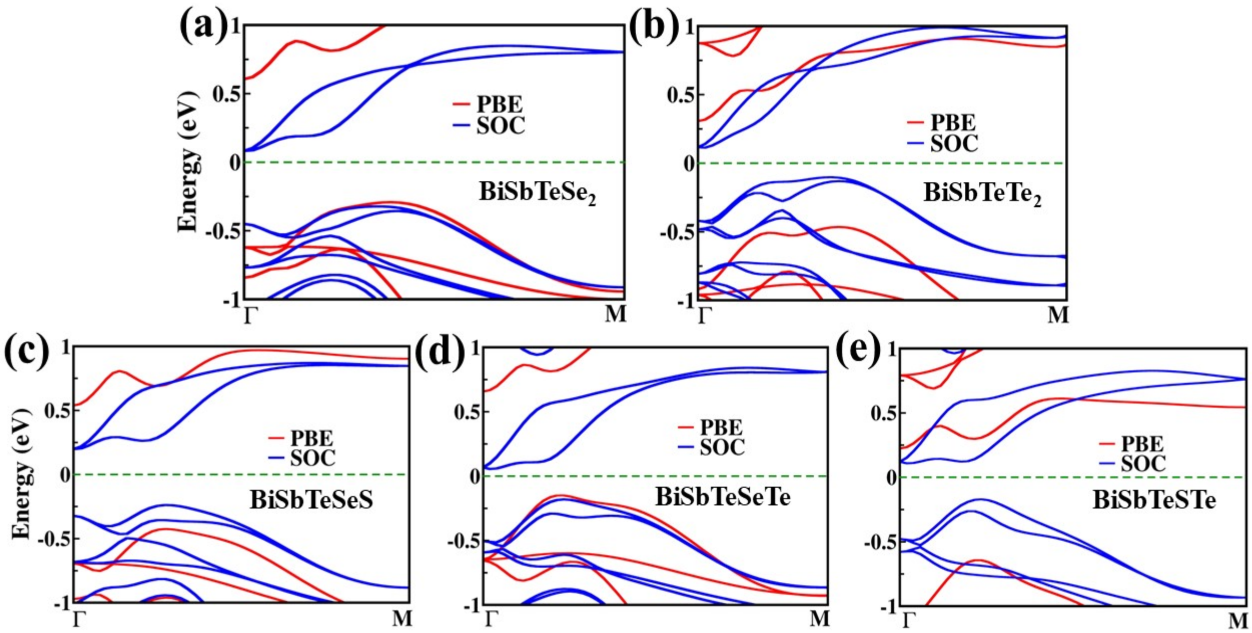

Fig. S19 The calculated band structure of **(a)** $BiSbTeSe_2$ **(b)** $BiSbTeTe_2$ and Janus **(c)** BiSbTeSeS, **(d)** BiSbTeSeTe**, (e)** BiSbTeSTe monolayers with PBE method (red color band) and PBE+SOC level (blue color band).

Table S4: Illustrations of ZT with PBE and PBE+SOC methods of $BiSbTeX_2$ (X=Se,Te) and Janus BiSbTeXY (X/Y = S, Se, Te) monolayers at 300 K temperature.

Materials	**(ZT)**			
	PBE		**PBE+SOC**	
	300 K	**500 K**	**300 K**	**500 K**
$BiSbTeSe_2$	0.72(p)-0.58(n)	1.31(p)-0.67(n)	1.37(p)-0.42(n)	1.99(p)-0.79(n)
$BiSbTeTe_2$	0.49(p)-0.09(n)	0.86(p)-0.22(n)	0.68(p)-0.14(n)	1.08(p)-0.31(n)
BiSbTeSeS	0.63(p)-0.39(n)	1.17(p)-1.08(n)	0.70(p)-0.40(n)	1.13(p)-0.67(n)
BiSbTeSeTe	0.52(p)-0.18(n)	0.85(p)-0.41(n)	0.35(p)-0.18(n)	0.88(p)-0.49(n)
BiSbTeSTe	0.59(p)-0.33(n)	0.86(p)-0.47(n)	0.55(p)-0.24(n)	1.01(p)-0.48(n)

Table S5: ZT of various 2D monolayers are listed here.

Materials	**Figure of Merit (ZT)**	**Temperature** (K)	**References**
Bi_2TeSe_2	0.87-3.45	300-900	[1]
Bi_2Te_2S **Bi_2Te_2Se** **Bi_2Te_3**	~ 0.6-0.8 ~ 0.6-0.8 ~ 0.6-0.8	300 -700	[2]

Bi_2Te_2Se	1.4- 2.0 (p)	300-500	3
Bi_2SSe_2 **Bi_2S_2Se**	0.50-0.28(p) 1.39- 0.93(p)	300-700	4
Bi_2Te_3 **$BiPTe_3$** **$BiSbTe_3$** **$BiAsTe_3$**	0.61 1.01 1.08 1.10	300	5
Sb_2Te_2Se **Sb_2Te_2Se**	1.28-2.28-2.98(p) 1.86-2.99-3.75(n)	300-500-700	6
WS_2 **Janus WSSe** **Janus WSTe**	0.006 0.013 0.742	300	7
WSe_2	0.138	300	8

Table S6: The calculated efficiency (η_{max}) with PBE and PBE+SOC methods of $BiSbTeX_2$ (X=Se,Te) and Janus BiSbTeXY (X/Y = S, Se, Te) monolayers . Also these monolayers is compare with other monolayers.

Materials	η_{max} **(%)**		**References**
	PBE	**PBE+SOC**	
$BiSbTeSe_2$	34(p)-33(n)	35(p)-32(n)	This work
$BiSbTeTe_2$	33(p)-26(n)	34(p)-30(n)	
BiSbTeSeS	33(p)-32(n)	34(p)-32(n)	
BiSbTeSeTe	33(p)-29(n)	30(p)-29(n)	
BiSbTeSTe	34(p)-31(n)	33(p)-30(n)	
X_2YH_2 (X=Si, Ge; Y=P, As, Sb, Bi)		18(p)-10(n)	9

References

1. N. Wang, C. Shen, Z. Sun, H. Xiao, H. Zhang, Z. Yin and L. Qiao, *ACS Applied Energy Materials*, 2022, **5**, 2564-2572.

2. Z. Rashid, A. S. Nissimagoudar and W. Li, *Physical Chemistry Chemical Physics*, 2019, **21**, 5679-5688.
3. N. T. Hung, A. R. Nugraha and R. Saito, *Nano Energy*, 2019, **58**, 743-749.
4. S.-H. Cao, T. Zhang, C.-E. Hu, X.-R. Chen and H.-Y. Geng, *Physical Chemistry Chemical Physics*, 2022, **24**, 26753-26763.
5. T. Li, J. Pu, T. Yu, Z. Hu and X. Shao, *New Journal of Chemistry*, 2023, **47**, 13309-13319.
6. Y. Chen, Y. Wu, B. Hou, J. Cao, H. Shao, Y. Zhang, H. Mei, C. Ma, Z. Fang and H. Zhu, *Journal of Materials Chemistry A*, 2021, **9**, 16108-16118.
7. A. Patel, D. Singh, Y. Sonvane, P. Thakor and R. Ahuja, *ACS applied materials & interfaces*, 2020, **12**, 46212-46219.
8. S. Kumar and U. Schwingenschlogl, *Chemistry of Materials*, 2015, **27**, 1278-1284.
9. M. A. Mohebpour, S. M. Mozvashi, S. I. Vishkayi and M. B. Tagani, *Scientific Reports*, 2021, **11**, 23840.